AGU ADVANCING EARTH AND SPACE SCIENCE

Earth and Space Science

RESEARCH ARTICLE
10.1029/2021EA001662

Key Points:

- Earthquake-spawning faults run across the Seoul metropolitan area
- Chugaryeong fault behaves as a single continuous fault, producing earthquakes
- Branch faults develop locally by the ambient stress field

Correspondence to:
T.-K. Hong,
tkhong@yonsei.ac.kr

Citation:
Hong, T.-K., Chung, D., Lee, J., Park, S., Kim, B., & Kim, W. (2021). Earthquake-spawning faults in the Seoul metropolitan area and their seismic implications. *Earth and Space Science*, *8*, e2021EA001662. https://doi.org/10.1029/2021EA001662

Received 12 JAN 2021
Accepted 1 JUN 2021

Earthquake-Spawning Faults in the Seoul Metropolitan Area and Their Seismic Implications

Tae-Kyung Hong[1], Dongchan Chung[1], Junhyung Lee[1], Seongjun Park[1], Byeongwoo Kim[1], and Woohan Kim[2]

[1]Department of Earth System Sciences, Yonsei University, Seoul, South Korea, [2]Department of Earth and Environmental Sciences and RINS, Gyeongsang National University, Jingu si, South Korea

Abstract Quaternary faults run across the Seoul metropolitan area that is the highest population region in the Korean Peninsula. Active fault identification and seismic hazard potential assessment are crucial for public safety. Densely deployed permanent and temporal seismic stations enabled us to detect micro to small earthquakes, allowing us to identify earthquake-spawning faults in Seoul metropolitan area. The source parameters of 455 earthquakes in 2004–2020 are refined. The Gutenberg-Richter *b* value is 0.94. Dominant focal depths are 4–15 km. The focal mechanism solutions of 64 earthquakes are determined using seismic-wave polarities and amplitude ratios. Strike-slip earthquakes are dominant in the region. Earthquakes are clustered around the Chugaryeong fault system. The dominant strikes of fault planes range from N20°E to N45°E in the northern and southern Seoul metropolitan areas, suggesting branch fault development locally. The earthquakes in middle-northern Seoul present N-S directional strike-slip motions at depths ~7.5 km along the Chugaryeong fault, suggesting seismically active near-vertical faults subparallel with Chugaryeong fault.

Plain Language Summary The Seoul metropolitan area is the largest population region in the Korean Peninsula. More than 20 million people live in the area where Quaternary faults run across. Historical literatures presented high seismic damages in the region. Active fault identification and seismic hazard potential assessment are crucial for public safety. Dense seismic stations were deployed to investigate the seismicity and earthquake-spawning faults in the Seoul metropolitan area. We refined the source locations of 455 earthquakes in 2004–2020. The focal mechanisms solutions of 64 earthquakes were determined using the seismic-wave polarities and amplitude ratios. Strike-slip earthquakes are dominant in the region. The strikes of fault planes range from N20°E to N45°E in the northern and southern Seoul metropolitan areas. Branch faults appear to develop locally according to the ambient stress field. Microseismicity are clustered locally. The earthquakes in middle-northern Seoul present N-S directional strike-slip motions at depths ~7.5 km along the Chugaryeong fault. The Chugaryeong fault system appears to be seismically active.

1. Introduction

The Korean Peninsula is located in a stable intraplate region with low seismicity. Tectonic stress is transmitted from active plate margins off the Japanese islands and Indo-Eurasian plate collision zone. The lithostatic stress is loaded continuously in the crust of the Korean Peninsula. The lithostatic stress is accumulated slowly in stable intraplate regions, producing earthquakes with long recurrence intervals (Pearthree & Calvo, 1987; Schwartz & Coppersmith, 1984; Shimazaki & Nakata, 1980).

The seismicity in the Korean Peninsula has increased since the 2011 M_W9.0 Tohoku-Oki megathrust earthquake (Hong et al., 2015; Hong, Park, Lee, Chung & Kim, 2020; Hong, Park, Lee & Kim, 2020). Moderate-size earthquakes occurred successively in the Korean Peninsula since the Tohoku-Oki earthquake (Hong et al., 2018). The moderate-size earthquakes include the September 12, 2016 M_L5.8 Gyeongju earthquake, which is the largest event since 1978 when national monitoring began. There is increasing concern regarding possible large earthquakes in the peninsula. There were seismic intensities reaching VII-IX according to historical seismic damages (Kyung, 2012; K. Lee & Yang, 2006; Park et al., 2020). There were large earthquakes in the Korean Peninsula, including the Seoul metropolitan area (Park et al., 2020).

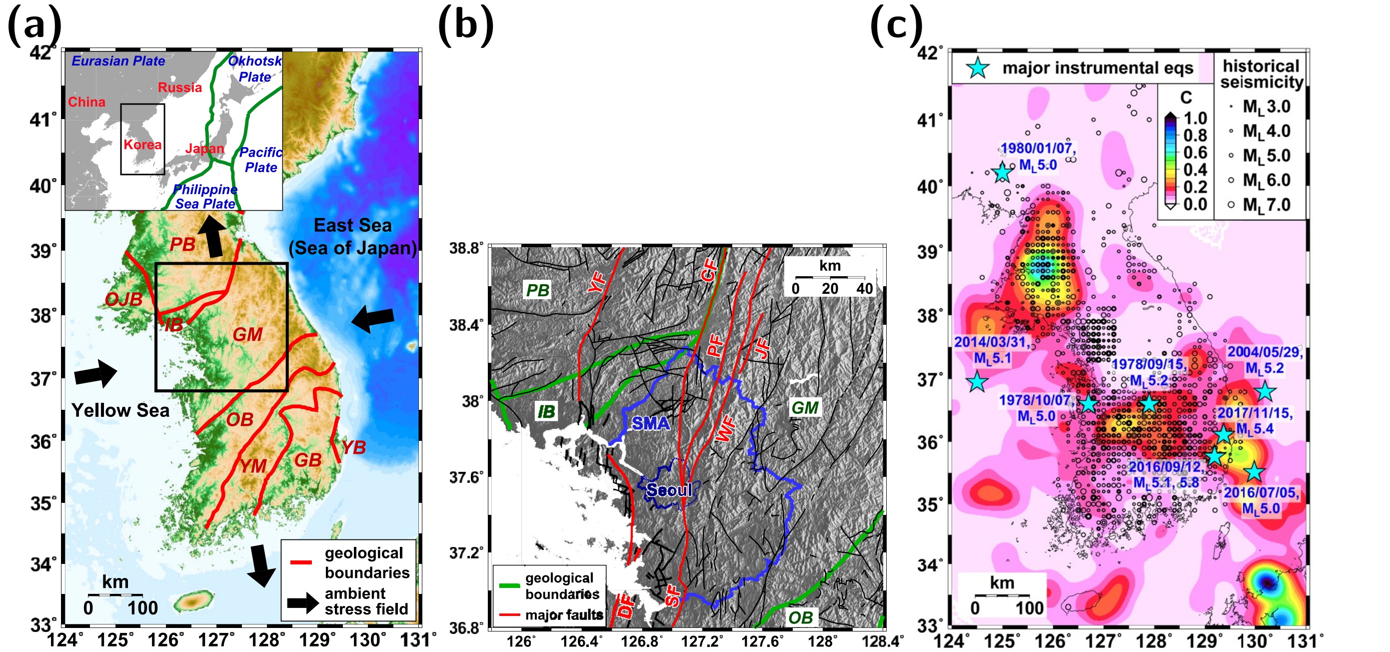

Figure 1. (a) Tectonic setting and major geological provinces. The ambient stress field is indicated by arrows. Major geological provinces include Gyeonggi massif (GM), Gyeongsang basin (GB), Imjingang belt (IB), Okcheon belt (OB), Ongjin basin (OJB), Pyeongnam basin (PB), Yeongnam massif (YM), and Yeonil basin (YB). (b) Major faults in the central Korean Peninsula and Seoul metropolitan area (SMA). Major faults include Chugaryeong fault (CF), Dangjin fault (DF), Jamgok fault (JF), Pocheon fault (PF), Singal fault (SF), Wangsukcheon fault (WF), and Yeseoggang fault (YF). (c) Instrumental seismicity densities, historical earthquakes, and major earthquakes with magnitudes ≥ M_L 5.0 since 1978 (stars). Index C presents the normalized instrumental seismicity density.

More than 20 million people live in the Seoul metropolitan area, which includes Seoul capital city and Gyeonggi province. The Seoul metropolitan area is the largest population region in the Korean Peninsula. Quaternary faults including the Chugaryeong fault are located in the Seoul metropolitan area (H. Choi et al., 2012; Chung et al., 2014). The presence of Quaternary faults raises public concerns regarding possible seismic damages in the Seoul metropolitan area (Kyung, 2012; Park et al., 2020).

According to instrumental earthquake records, the seismicity is low around the Seoul metropolitan area. However, historical seismic-damage records suggest the occurrence of devastating earthquakes in the region (Houng & Hong, 2013; Kyung, 2012; Park et al., 2020). The magnitudes of large historical earthquakes might be as large as ~M_L6.8 (Park et al., 2020). The historical earthquakes suggest a possible presence of active faults in the region. However, the distribution of active faults is poorly known. Furthermore, there is a lack of understanding of subsurface fault activation. We investigate active faults and their geometry using focal mechanism solutions and event distribution. This study provides information on the fault structure in the central peninsula, including the Seoul metropolitan area. The information may be used for mitigation of seismic hazards in the regions.

2. Data and Geology

The Korean Peninsula is located near the eastern margin Eurasian plate (Figure 1). The Philippine Sea plate and the Okhotsk plate collide with the Eurasian plate, producing a stress field of ENE-directed compression and WNW-directed tension over the Korean Peninsula (S.-J. Choi et al., 2012; J. Lee et al., 2017). Major geological provinces are composed of three Precambrian massif blocks (Gyeonggi massif, Yeongnam massif, Pyeongnam massif) and two intervening belts (Okcheon belt, Imjingang belt) (Chough et al., 2000). The crustal thicknesses are 29–36 km (He & Hong, 2010; Hong et al., 2008). Gyeonggi massif and Imjingang belt comprise the central Korean Peninsula, where the population is high (Figure 1). The Gyeonggi massif region is a seismically quiescent region in the Korean peninsula.

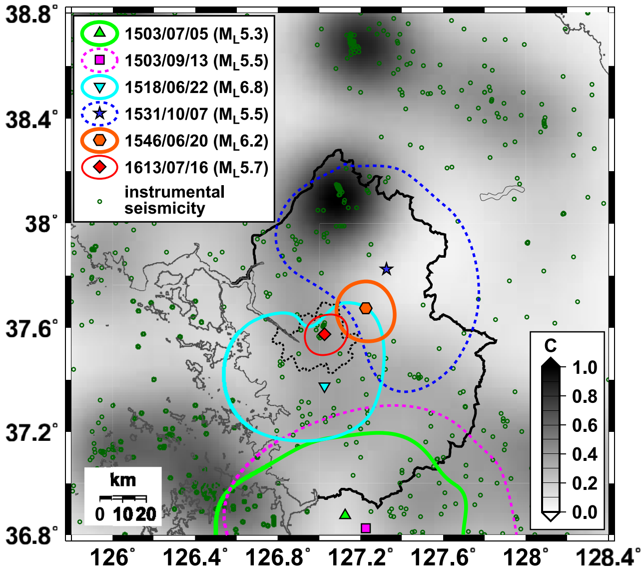

Figure 2. Normalized instrumental seismicity densities (shaded) and possible locations of major historical earthquakes. The epicenters of instrumentally observed earthquake locations are indicated (dots). Relatively high seismicity densities are observed in the northern Seoul metropolitan area. The major historical earthquake locations partly overlap with high seismicity regions.

Quaternary faults exist in the central Korean Peninsula. The Chugaryeong fault system is a primary fault system in the region. The Chugaryeong fault system is composed of Chugaryeong (Daeseongri), Pocheon, Wangsukcheon, and Singal faults with NNE and NE orientations (Bae & Lee, 2016; H. Choi et al., 2012; Chung et al., 2014; O. J. Kim, 1973) (Figure 1). The faults present apparent lineaments on the surface. The Chugaryeong fault runs from Weonsan through Seoul to southern Gyeonggi province. The fault may reach Boryeong, Choongnam (H. Choi et al., 2012).

The ambient stress field is composed of ENE-WSW directional compression and NWN-SES directional tension. The ambient stress field produces strike-slip earthquakes with dominant NE-SW fault-plane orientations in the Korean Peninsula (Hong & Choi, 2012). The instrumentally observed seismicity is low in the central Korean Peninsula around the Seoul metropolitan area (Hong et al., 2016) (Figure 1). The recurrence intervals of earthquakes are large.

Previous studies report devastating historical earthquakes in the Korean Peninsula (Kyung, 2012; Park et al., 2020). The historical seismicity displays high similarity with the instrumental seismicity (Hong et al., 2018; Houng & Hong, 2013; Park et al., 2020) (Figure 1c). However, we find apparent difference between historical and instrumental seismicity in the Seoul metropolitan area. There were 61 historical earthquakes in the Seoul metropolitan area during the Joseon dynasty from 1392 to 1910 (Houng & Hong, 2013; K. Lee & Yang, 2006).

In particular, six earthquakes with magnitudes of M_L5.3–6.8 occurred around the Seoul metropolitan area during the Joseon dynasty (Park et al., 2020) (Figure 2). The earthquakes occurred on July 5, 1503, September 13, 1503, June 22, 1518, October 7, 1531, June 20, 1546, and July 16, 1613. The event location of the July 16, 1613 earthquake is well constrained to be placed in the northern Seoul. The seismic intensities of large historical earthquakes reached VIII–IX in the modified Mercalli intensity (MMI) scale (Kyung, 2012; Park et al., 2020). Such large seismic intensities may occur with recurrence periods of 1,400–1,500 years (Kyung, 2012). Earthquakes with long recurrence intervals may not be well represented in the instrumental seismicity that is based on the earthquake records since 1978.

There were 10 events with magnitudes $M_L \geq 5.0$ in the Korean Peninsula since 1978 (Figure 1). The M5-level earthquakes occur in the outskirts of high seismicity regions (Figure 1). Moderate-size earthquakes increased after the March 11, 2011 M_W9.0 Tohoku-Oki earthquake (Hong et al., 2018). The September 12, 2016 M_L5.8 Gyeongju earthquake is the largest event since 1978, when national seismic monitoring began. The Gyeongju earthquake was a mid-crustal event that occurred in a junction to the main fault, Yangsan fault. The fault plane and focal mechanism respond to the current ambient stress field (Hong et al., 2017; J. Lee et al., 2017).

The Tohoku-Oki earthquake affected offshore seismicity as well as inland seismicity (Hong, Park, Lee & Kim, 2020). Shallow to mid-crustal earthquake swarms started to occur in the Korean Peninsula after the Tohoku-Oki earthquake (Hong et al., 2015, Hong, Park, Lee, Chung & Kim 2020). This observation suggests that the medium or stress field perturbation by the Tohoku-Oki earthquake produces frequent earthquake occurrence and deep-focus earthquake swarms. The deep-focus earthquake swarms may imply possible occurrence of major earthquakes at deeper depths. The earthquakes in deeper depths may require large accumulations of stress, which may take a longer time as compared to events in shallower depths. The historical and instrumental earthquakes may suggest the possible occurrence of major earthquakes in the Seoul metropolitan region.

A dense seismic network is available around the Seoul metropolitan area. The network is composed of permanent stations and temporal stations that are equipped with broadband, short-period sensors or accelerometers (Figure 3). The sampling rates are 20–200 Hz. The temporal stations have operated since September

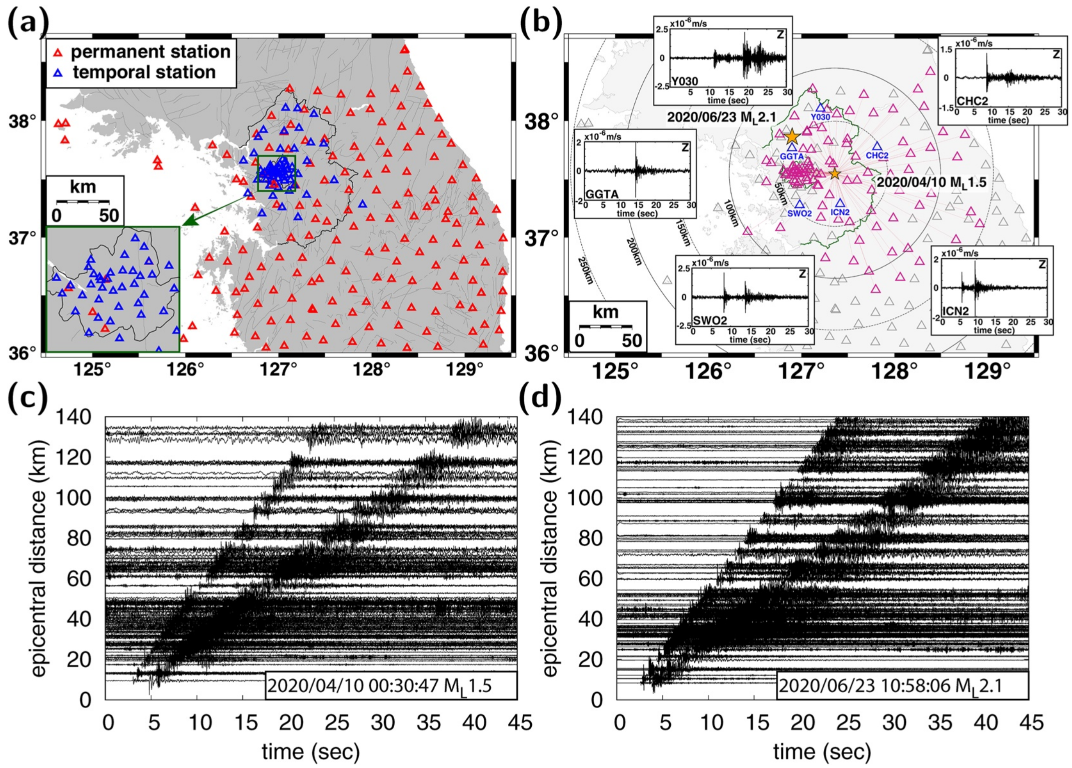

Figure 3. (a) Distribution of seismic stations in the central Korean Peninsula. Example of event detection in Seoul metropolitan area: (b) map and enlarged waveform, as well as seismic waveforms for (c) the April 10, 2020 M_L1.5 earthquake and (d) the June 23, 2020 M_L2.1 earthquake. The seismic waveforms are filtered to within 1.0–10 Hz.

2018 to monitor the seismic activity around the Seoul metropolitan area. The dense seismic stations allow us to detect micro to small events in local distances. We investigate the earthquakes in 2004–2020 in the region with latitudes of 36.8°N–38.8°N and longitudes of 125.8°E–128.4°E.

We collect seismic data from 170 permanent stations from the Korean Meteorological Administration (KMA) and Korea Institute of Geoscience and Mineral Resources (KIGAM), and 61 stations temporally deployed around the Seoul metropolitan area (Figure 3).

3. Method

Earthquakes are detected using seismic records from local seismic networks. Earthquakes are detected based on a short-time average over long-time average (STA/LTA) of waveform amplitudes (Withers et al., 1998). We determine the hypocentral parameters of earthquakes using a source-parameter inversion method, VELHYPO, which jointly inverts the hypocentral parameters and velocity structures (W. Kim et al., 2014, 2016). The method can be applicable to regions with unknown velocity structures (W. Kim et al., 2016). We further refine the event locations using a double-difference method (hypoDD) when the earthquakes are clustered in small regions (Waldhauser & Ellsworth, 2000). Here, we measure the traveltime differences with respect to reference waveforms at stations.

The seismicity generally satisfies the Gutenberg-Richter magnitude-frequency relationship (Gutenberg & Richter, 1956):

$$\log N = a - b \cdot M, \tag{1}$$

where M is the magnitude, N is the number of earthquakes with magnitudes greater than or equal to M, and a and b are constants.

The focal mechanism solution presents the geometry of fault plane and faulting sense. We determine the focal mechanism solutions of small earthquakes based on the phase polarity and amplitudes (FOCMEC) (Snoke, 2003). The focal mechanism solution inversion based on the phase polarity and amplitudes yields stable results for general velocity models. We use a global 1-D velocity model (ak135) (Kennett et al., 1995). The *P* and *S* phases are searched considering the theoretical traveltimes of *P* and *S* waves based on the 1-D velocity model. When the focal mechanism solutions are poorly constrained with *P* and *S* polarities, we additionally use phase amplitude ratios.

We identify the fault type using the dip angles of primary stress components from focal mechanism solutions (Frohlich & Apperson, 1992). We define strike-slip events to have null-axis (*B*-axis) dip angles of ≥60°. Normal-faulting events have compression-axis (*P*-axis) dip angles of ≥60°. Thrust events have tension-axis (*T*-axis) dip angles of ≥50°. We classify the earthquakes satisfying none of these criteria to be events of complex mechanisms that can be represented by combinations of two or three fault types.

We measure the moment magnitude using coda waves in velocity record sections that are corrected for instrument responses. The coda envelope (amplitude) is given by (Mayeda & Walter, 1996; Yoo et al., 2011)

$$A_C(t,f,r) = W_0(f)S(f)P(f,r)E(t,f,r), \tag{2}$$

where $W_0(f)$ is the *S* wave source amplitude at frequency *f*, $S(f)$ is the site amplification and coda transfer function, $P(f, r)$ accounts for geometrical spreading and attenuation during propagation, and $E(t, f, r)$ is the coda envelop function for frequency *f* at time *t* and distance *r*.

The source spectral amplitude is given by

$$W_0(f) = \frac{M_0}{1 + (f / f_c)^2}, \tag{3}$$

where M_0 is the seismic moment, and f_c is the corner frequency. The coda envelop function is given by

$$E(t,f,r) = H\left[t - \frac{r}{v(f,r)}\right]\left(t - \frac{r}{v(f,r)}\right)^{-\gamma(f,r)} \exp\left[b(f,r)\left(t - \frac{r}{v(f,r)}\right)\right], \tag{4}$$

where *H* is the Heaviside step function, *v* is the velocity, and $\gamma(f, r)$ and $b(f, r)$ control the coda decay rates.

We calculate the source spectra after correction of path effects in the spectral amplitudes. We determine the amplitudes of source spectra by frequency (Yoo et al., 2011). We choose two frequency bands for which source spectral amplitudes are well determined. The station correction term calibrates the amplitudes for site effects. We use the station correction terms of nearby stations (Yoo et al., 2011). We determine the coda moment magnitude M_W(coda) using the average values of the source spectral amplitudes of two frequency bands (Mayeda & Walter, 1996). We determine the moment magnitude based on the seismic moments (Hanks & Kanamori, 1979).

4. Analysis

We analyze the seismicity in the region with latitudes of 36.8°N–38.8°N and longitudes of 125.8°E–128.4°E (Figure 4). Earthquakes in the region were well monitored by the local and regional seismic stations (Figure 3). The seismic waveforms present clear phase arrivals in local and near-regional distances. We refine the hypocenters and origin times of 455 earthquakes in 2004–2020 using VELHYPO based on *P* and *S* arrival times in local networks (W. Kim et al., 2014, 2016).

Seismic stations are densely located in the Seoul metropolitan area. The numbers of stations used for event refinement range between 4 and 82, with 5–20 for most cases (Figure 4). The average number of stations is 12. The horizontal and vertical source location errors are less than 0.55 and 1.08 km at 95% confidence level. We refined the source parameters of 64 earthquakes in 2004–2020 around the Seoul metropolitan area (Table 1).

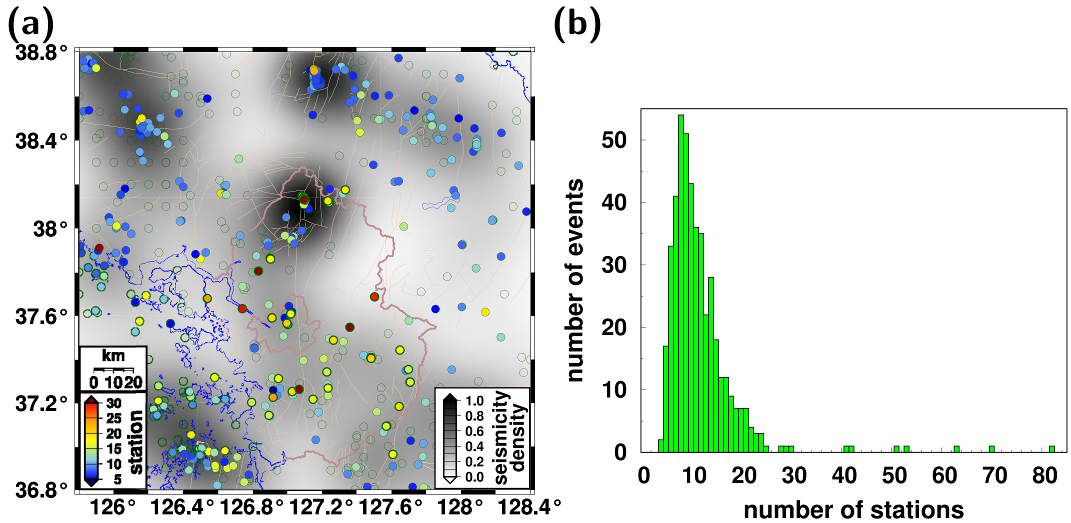

Figure 4. (a) Numbers of stations used for event relocation. Event locations (circles) and seismicity densities (shaded) are presented. (b) Histogram for the number of events as a function of number of stations used for event relocation.

We determine the magnitudes of events based on the coda amplitudes in horizontal components (Figure 5). The horizontal amplitudes, u_H, of waveforms are determined by

$$\log u_H = \frac{1}{2}\left(\log u_E + \log u_N\right), \tag{5}$$

where u_E and u_N are the waveform amplitudes in EW and NS components. We consider 13 frequency bands of 0.3–0.5 Hz, 0.5–0.7 Hz, 0.7–1.0 Hz, 1.0–1.5 Hz, 1.5–2.0 Hz, 2.0–3.0 Hz, 3.0–4.0 Hz, 4.0–6.0 Hz, 6.0–8.0 Hz, 8.0–10.0 Hz, 10.0–15.0 Hz, 15.0–20.0 Hz, and 20.0–25.0 Hz.

We first correct the coda amplitudes for the site effects (site amplification and coda transfer function) and path effects (geometrical spreading effect and attenuation during propagation). The site effects are corrected by station. We adopt known site correction terms of nearby stations to correct the site effects at stations (Yoo et al., 2011). We correct for the geometrical spreading effect and regional seismic attenuation (Mayeda et al., 2003; Yoo et al., 2011). The corrected coda amplitudes are fitted with theoretical coda-envelop curves by frequency band (Figure 5a–5c). The levels of coda envelopes represent the *S* wave source amplitudes.

We determine the seismic moments from the *S* wave source amplitudes. The moment magnitudes are determined by frequency band using the seismic moments (Mayeda & Walter, 1996). We choose the results for two frequency bands where the curves fit best with the observed spectra (Figure 5d–5f). Micro and small earthquakes generally fit well in frequencies of 6–25 Hz. We additionally estimate the local magnitude for undetermined events using the *S* wave source amplitudes (Yoo et al., 2011) (Table 1). The local magnitudes and moment magnitudes are determined close.

We find that the estimated moment magnitude based on coda waves are comparable to the reported local magnitudes from the Korean Meteorological Administration (KMA) (Table 1). Also, the moment magnitudes based on coda waves are close to those from long-period waveform inversion. The moment magnitude estimates based on long-period waveform inversion for the September 21, 2019 and May 11, 2020 earthquakes (events #50 and #61 in Table 1) are M_W3.5 and 3.6 that are close to those based on coda waves.

We determine the focal mechanism solutions of 64 earthquakes using the waveforms recorded at local and regional stations. Focal mechanism solutions from previous studies are combined together (S.-J. Choi, et al., 2012; Hong & Choi, 2012).

Table 1
Source Information of Earthquakes Analyzed for Focal Mechanism Solutions

No	Date (yyyy/mm/dd)	Time (hh:mm:ss)	Lat (°N)	Lon (°E)	Dep (km)	M_L	M_W (coda)	Plane 1 $\phi/\delta/\lambda(°)$	Plane 2 $\phi/\delta/\lambda(°)$	N_S	id
1	2004/09/14	22:47:33.5	37.452	126.811	12.1	2.5[a]	2.4	109/80/1	19/89/170	15	R3-15
2	2009/03/26	13:21:25.0	38.109	127.095	8.1	2.7[a]	3.1	300/88/-9	30/80/-178	30	R2-6
3	2009/06/05	15:49:43.0	38.605	127.423	4.0	2.8[a]	2.6	301/83/-24	34/65/-173	22	R1-6
4	2010/10/08	19:40:10.6	37.395	127.092	9.2	1.5[a]	2.3	120/77/15	26/74/166	22	R3-13
5	2011/03/11	00:57:55.9	38.519	127.585	9.0	2.5[a]	2.8	134/81/5	43/85/171	13	R1-8
6	2011/11/02	17:54:15.9	37.217	127.147	8.1	1.5[a]	2.2	310/51/34	197/63/135	27	
7	2012/07/20	15:20:02.1	37.937	126.884	10.9	1.1[a]	1.5	230/45/-90	50/45/-90	11	R2-3
8	2013/11/02	09:11:05.0	38.159	127.319	9.0	1.8[a]	2.1	115/78/-9	207/80/-168	21	R2-14
9	2013/11/25	17:26:02.6	37.124	128.113	11.9	2.1[a]	2.6	285/88/4	194/85/178	35	
10	2013/12/19	03:38:25.1	38.145	127.085	7.1	2.9[a]	2.9	115/80/17	22/72/169	31	R2-7
11	2014/08/01	16:32:27.5	37.403	127.208	14.5	2.2[a]	2.6	303/63/44	189/51/145	27	R3-12
12	2014/09/28	12:32:44.5	37.225	126.447	8.2	3.2[a]	3.7	91/86/9	0/80/176	33	
13	2015/03/11	07:35:58.5	37.202	126.793	12.2	1.1[a]	1.9	314/85/-1	45/88/-175	20	
14	2015/08/11	15:51:04.0	37.963	127.035	5.6	1.3[a]	1.7	313/74/-19	48/71/-163	17	R2-4
15	2015/08/12	08:09:51.3	37.159	127.514	13.6	2.2[a]	2.4	254/66/-26	355/66/-153	19	
16	2016/04/15	08:54:37.0	37.084	128.328	8.9	1.6[a]	1.7	315/80/-1	45/88/-170	15	
17	2016/06/16	09:11:35.8	36.910	126.688	9.0	1.9[a]	2.1	120/85/2	29/87/175	17	
18	2016/08/20	03:18:21.7	38.392	128.088	5.4	3.0[a]	3.0	140/75/-3	231/86/-165	30	
19	2016/10/24	00:02:02.1	37.252	127.027	7.6	2.2[a]	2.6	117/81/12	25/77/171	37	R3-14
20	2017/01/29	04:45:54.2	38.701	127.150	7.0	2.6[a]	2.6	119/85/-2	210/87/-175	24	R1-4
21	2017/03/24	18:52:07.7	38.139	127.089	9.2	1.9[a]	2.0	289/86/-14	20/75/-176	29	R2-8
22	2017/04/04	03:23:02.8	37.312	126.947	16.4	1.7[a]	2.0	106/81/5	15/85/171	17	R3-1
23	2017/06/03	20:16:11.6	36.831	128.103	18.6	2.1[a]	2.2	98/80/-1	188/89/-170	22	
24	2017/12/23	18:25:39.4	37.092	127.568	8.1	1.3[a]	1.3	115/85/2	24/87/175	17	
25	2018/04/15	12:03:23.2	37.443	127.648	4.6	1.7[a]	1.7	134/88/-4	225/85/-178	32	
26	2018/06/28	09:43:00.4	38.175	127.333	8.8	2.7[a]	2.8	305/81/5	214/84/171	43	R2-13
27	2018/07/03	19:39:40.7	37.296	127.706	10.7	2.1[a]	2.1	108/85/8	18/81/174	41	
28	2018/07/13	14:17:06.7	37.294	127.707	12.2	1.0[a]	1.5	312/42/67	161/51/109	13	
29	2018/09/24	00:21:44.4	38.671	127.171	7.6	1.6[a]	2.1	304/89/-4	35/85/-179	16	R1-1
30	2018/10/12	07:43:00.4	38.693	127.161	11.4	2.3[a]	2.3	307/80/1	217/88/170	21	R1-3
31	2018/11/03	14:54:45.2	38.008	127.670	4.2	1.7[a]	1.9	64/90/160	154/70/-1	13	
32	2018/11/26	16:38:46.3	37.989	127.081	4.7	1.3[a]	1.2	118/73/-11	211/78/-163	13	R2-5
33	2018/12/16	19:59:47.0	37.687	127.502	9.3	1.8[a]	1.8	284/87/-14	15/75/-177	40	
34	2019/01/07	22:21:54.8	37.488	127.265	8.9	1.2[a]	1.4	66/84/-14	158/75/-174	21	R3-10
35	2019/01/13	12:09:20.8	37.018	127.927	16.4	2.0[a]	2.2	97/74/-19	192/71/-163	31	
36	2019/01/29	23:06:58.2	37.607	127.019	7.4	1.5[a]	1.7	98/60/28	353/65/147	17	R3-4
37	2019/02/05	05:10:59.0	37.610	127.023	7.7	1.3[a]	1.6	97/68/34	352/58/154	15	R3-5
38	2019/03/18	20:31:06.8	38.011	126.016	15.0	2.2[a]	2.3	72/60/-84	241/30/-99	32	
39	2019/03/19	05:02:56.9	37.611	127.021	8.4	1.5	1.9	106/76/6	14/83/166	21	R3-7
40	2019/03/20	23:14:26.6	37.609	127.019	7.3	1.5	1.9	97/77/8	5/81/167	17	R3-6
41	2019/04/14	08:37:25.7	37.295	127.706	10.6	0.7[a]	1.7	284/86/9	194/80/176	26	
42	2019/04/21	08:59:19.5	38.604	127.584	9.5	2.0	2.5	240/25/-90	60/65/-90	28	R1-7
43	2019/05/10	02:59:24.0	38.436	127.418	7.7	2.2	2.6	228/30/-80	37/60/-95	42	R1-9

Table 1
Continued

No	Date (yyyy/mm/dd)	Time (hh:mm:ss)	Lat (°N)	Lon (°E)	Dep (km)	M_L	M_W (coda)	Plane 1 $\phi/\delta/\lambda$(°)	Plane 2 $\phi/\delta/\lambda$(°)	N_S	id
44	2019/06/25	21:39:17.7	37.641	128.004	12.4	1.8[a]	2.4	294/88/9	204/80/178	42	
45	2019/07/14	13:49:25.8	37.496	127.240	10.6	0.8[a]	1.4	308/81/-12	40/77/-171	14	R3-9
46	2019/07/16	18:21:35.2	37.482	127.322	9.8	0.9[a]	1.2	128/81/-5	219/85/-171	28	R3-11
47	2019/08/02	16:00:46.2	36.962	127.607	16.1	1.0[a]	1.1	115/80/17	22/72/169	31	
48	2019/09/10	19:52:08.2	38.130	127.101	8.8	2.0[a]	2.3	115/76/14	21/76/165	48	R2-11
49	2019/09/17	15:55:09.9	38.133	127.096	9.4	1.3[a]	1.8	113/90/15	23/75/180	18	R2-10
50	2019/09/21	06:11:16.7	38.678	127.163	8.5	3.5[a]	3.3	133/89/9	43/80/179	53	R1-2
51	2019/09/25	19:58:46.3	38.136	127.094	9.5	1.2[a]	1.2	108/83/13	16/76/173	29	R2-9
52	2019/11/08	11:11:11.9	38.126	127.103	8.0	1.3[a]	1.6	115/84/19	23/70/174	17	R2-12
53	2019/12/04	00:55:55.3	36.898	126.653	13.8	1.8[a]	1.9	275/86/-19	7/70/-176	28	
54	2019/12/05	20:52:04.8	37.591	126.911	3.0	1.1[a]	1.2	109/86/-3	200/86/-176	25	R3-2
55	2019/12/05	22:53:27.3	37.590	126.911	3.1	1.0[a]	1.3	115/85/2	24/87/175	21	R3-3
56	2019/12/15	05:15:41.0	37.169	126.228	9.0	2.0[a]	2.3	289/66/-26	30/66/-153	32	
57	2020/01/14	16:36:41.7	37.110	128.285	9.9	1.9[a]	2.0	290/86/-19	21/70/-176	45	
58	2020/01/15	13:46:11.7	37.111	128.284	10.0	2.1[a]	2.1	290/81/-18	22/71/-171	38	
59	2020/01/24	08:38:07.2	37.053	126.445	11.1	1.9[a]	2.0	292/80/-1	22/89/-170	30	
60	2020/04/10	00:30:47.5	37.548	127.359	11.5	1.5[a]	1.9	108/83/-7	199/82/-173	63	R3-8
61	2020/05/11	10:45:06.6	38.721	127.151	6.6	3.8[a]	3.5	134/86/19	43/70/176	130	R1-5
62	2020/05/30	06:22:59.5	37.508	126.977	4.1	1.3	1.6	300/81/5	210/85/171	22	
63	2020/06/23	10:58:05.8	37.863	126.901	6.2	2.1[a]	2.4	110/74/13	16/77/164	96	R2-2
64	2020/09/04	01:27:38.3	37.805	126.833	8.4	1.6[a]	1.7	299/70/5	207/84/160	47	R2-1

Note. Origin times, hypocenters, local magnitudes (ML), moment magnitudes (MW), fault plane solutions with strikes (ϕ), dips (δ), rakes (λ), numbers of stations used for focal-mechanism inversions (NS), and events in subregions are indicated.
[a]Local magnitudes (M_L) from Korean Meteorological Administration (KMA).

5. Average Velocity Model

The hypocentral parameter inversion method yields the seismic velocity models for the regions. We determine the average velocity model for the central Korean Peninsula (Figure 6). The ray path coverage supports the representative velocity model from the joint inversion. We compare the velocity model with other studies (Hong et al., 2018; Kennett et al., 1995; W. Kim et al., 2011). The global 1-D velocity (ak135) was inverted from global travel seismic phases (Kennett et al., 1995).

A 1-D velocity model is inverted from receiver function analysis for Gyeongsang massif region (W. Kim et al., 2011). A regional velocity model for the southeastern peninsula was obtained from joint source-parameter and velocity model inversion based on local seismic phase arrival times (Hong et al., 2018). The inverted crustal velocity model is higher than the global average 1-D model or regional average 1-D model. On the other hand, the velocity model presents higher velocities than other models, and is slower than the local velocity model for the southeastern peninsula.

6. Seismicity and Hypocentral Parameters

The focal depths of the refined events are 1–38 km (Figure 7). Most events occurred at depths of 4–15 km (86%), which is consistent with typical focal depths observed in the Korean Peninsula (Hong et al., 2016). The magnitudes were M_L0.7–3.8 (Figure 7, Table 1). We determine the *b* value based on the refined seismicity since 2010 in which newly found events are included. We find the *b* value to be 0.94 (Figure 8). The minimum magnitude ensuring the event catalog completeness is M_L1.5 (Figure 8).

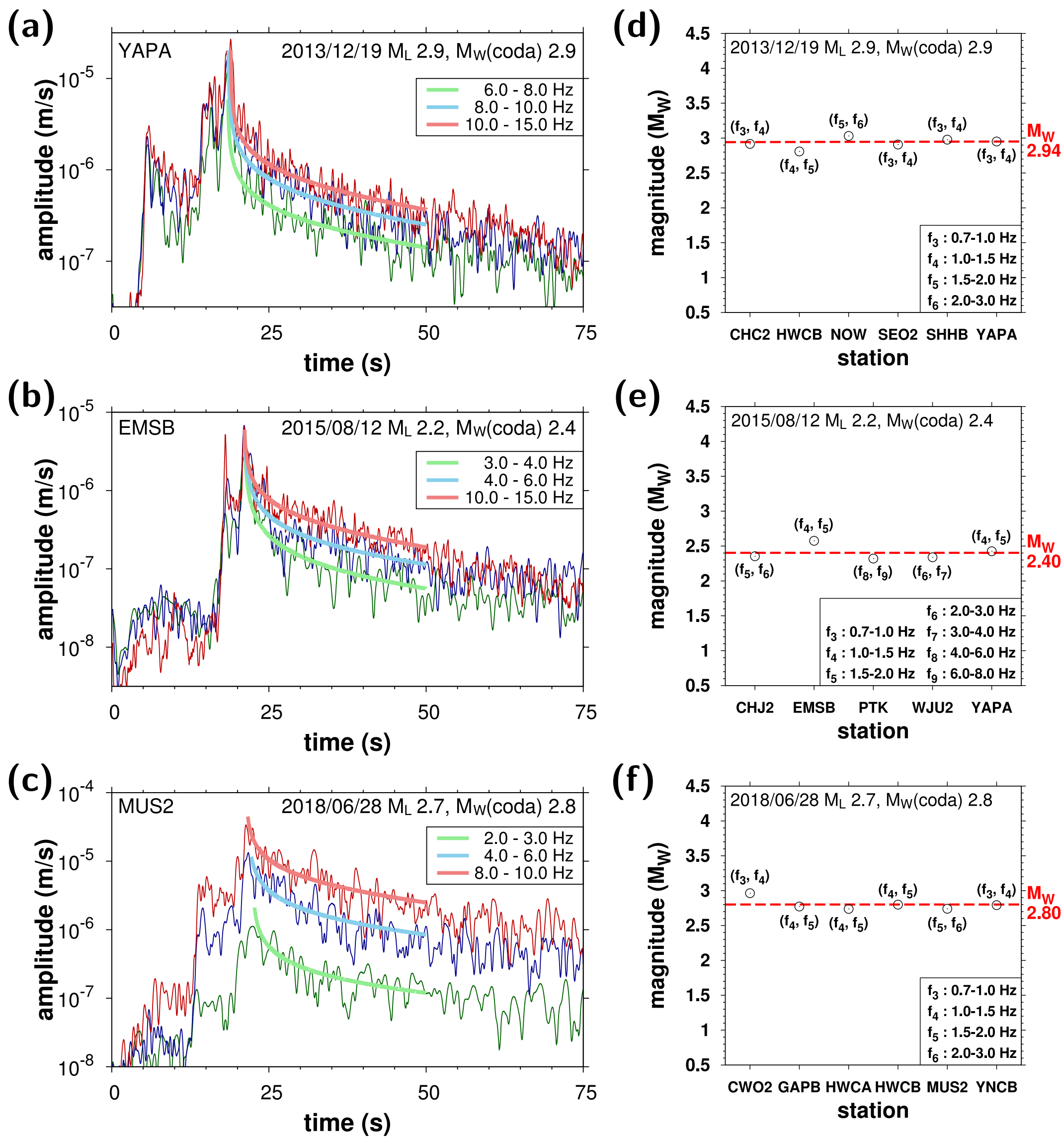

Figure 5. Examples of logarithmic horizontal waveform amplitudes for (a) the December 19, 2013 M_L2.9 earthquake at station YAPA, (b) the August 12, 2015 M_L2.2 earthquake at station EMSB, and (c) the June 28, 2018 M_L2.7 earthquake at station MUS2 in various frequency bands. Resultant moment magnitudes for (d) the December 19, 2013 M_L2.9 earthquake (e) the August 12, 2015 M_L2.2 earthquake, and (f) the June 28, 2018 M_L2.7 earthquake. The coda wavetrains of various frequency bands are fitted with theoretical curves (solid lines). The moment magnitudes by station and used frequency bands are indicated.

It is noteworthy that the *b* value for the seismicity in 1978–2020 is 0.81. Thus, the *b* value exceeds the average *b* value based on reported seismicity in the region since 1978 (Hong et al., 2016). This observation suggests that small earthquakes were better monitored with respect to recent seismicity.

The refined events are placed around surface lineaments (Figure 4). This observation suggests that some lineaments are associated with active faults. The vertical distribution of events suggests a vertical development of fault segments between 4 and 15 km (Figure 9). The seismicity densities present the earthquake clustering in the region (Figure 2). We analyzed the earthquakes since 1978. The seismicity density is relatively high in the northern Seoul metropolitan area. Also, the seismicity is relatively high in the region off the west coast of the southern Seoul metropolitan area.

10.1029/2021EA001662

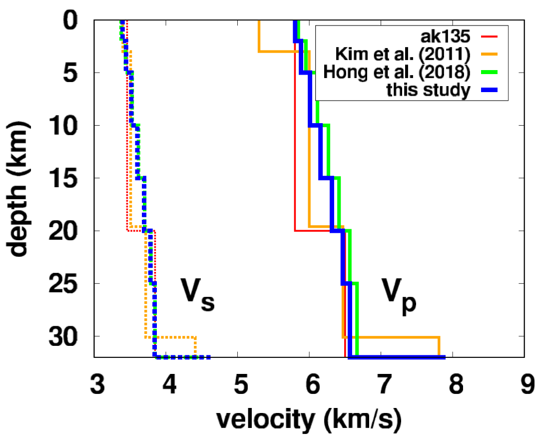

Figure 6. Inverted average 1-D velocity model for the central Korean Peninsula and comparison with other models. A global 1-D model (Kennett et al., 1995) and two local velocity models (Hong et al., 2018; Kim et al., 2011) are presented for comparison.

It is intriguing to note that major historical earthquakes rarely overlap with the spatial distribution of instrumental seismicity (Figure 2). The magnitudes of historical earthquakes are M_L5.3–6.8 at the locations of highest probabilities (Park et al., 2020). Major earthquakes occurred in low seismicity regions. In particular, the June 22, 1518 earthquake, the June 20, 1546 earthquake, and the July 16, 1613 earthquake might have occurred in the Seoul region. Observations suggest that major earthquakes may occur after long-term stress accumulation.

7. Focal Mechanism Solutions

The seismic waveforms and their polarities are well identified in local seismic stations (Figure 3). Also, the azimuthal coverage is generally good for local events (Figures 11–14). The focal mechanism solutions are well determined based on the phase polarities and amplitudes. The focal mechanism solutions of 64 earthquakes are determined. We used 11–130 stations for polarity analysis of events, with the average number of stations being 30.

We found 53 strike-slip earthquakes, five normal-faulting earthquakes, and four thrust earthquakes. We found two earthquakes with odd mechanisms (Figure 10). The focal mechanism solutions are combined with those from other studies (S.-J. Choi, et al., 2012; Hong & Choi, 2012). The determined focal mechanism solutions are consistent with previous observations (S.-J. Choi, et al., 2012; Hong & Choi, 2012). Strike-slip earthquakes are dominant in the region. The dominant strikes are within N20°E–N45°E, which is consistent with the general features of the peninsula (Hong et al., 2015). We use the focal mechanism solutions and event distribution to infer the fault structures at depths in the Seoul metropolitan area. The fault-plane orientation from focal mechanism solutions and event distribution generally agree with the surface fault traces in subregions (Figures 12–14).

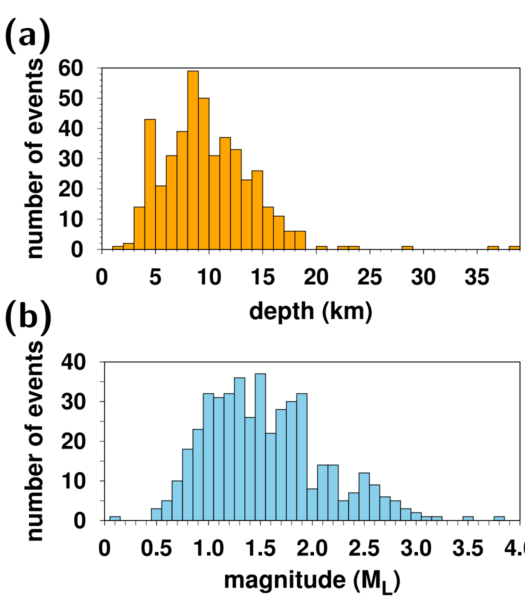

Figure 7. (a) Histograms for the numbers of events as a function of focal depth and (b) for those as a function of magnitude (M_L). The dominant focal depths are 4–15 km. The small and micro events are observed in the region.

8. Regional Features

We divide the study regions by three representative subregions along the Chugaryeong fault system (Figure 11). We investigate three subregions (R1, R2, R3) of the central Korean Peninsula around the Chugaryeong fault system (Figures 12–14). The spatial distribution of earthquakes and focal mechanism solutions present possible relationships with known faults on the surface (H. Choi et al., 2012). The refined seismicity and focal mechanism solutions may provide crucial information on the seismotectonic properties in the region. Most focal mechanism solutions present strike-slip earthquakes with strikes within N35°E–N45°E.

8.1. Region R1: Northeastern Chugaryeong Fault Zone

The northeastern Chugaryeong fault zone is composed of subparallel faults striking NEN-SWS (region R1; Figure 12). A part of the region belongs to North Korea. The earthquakes are clustered in the northern region that corresponds to a high seismicity region in the central Korean Peninsula. The earthquakes are generally clustered around fault traces including Chugaryeong fault (CF), Pocheon fault (PF), and Wangsukcheon fault (WF). Earthquakes are clustered most to the west of CF. This clustered seismicity illuminates fault trending in NE and SW.

The spatial distribution of earthquakes and surface fault traces present an apparent NNW lineament. The focal mechanism solutions in the northern region present strike-slip events striking in NE or NW. The fault-plane

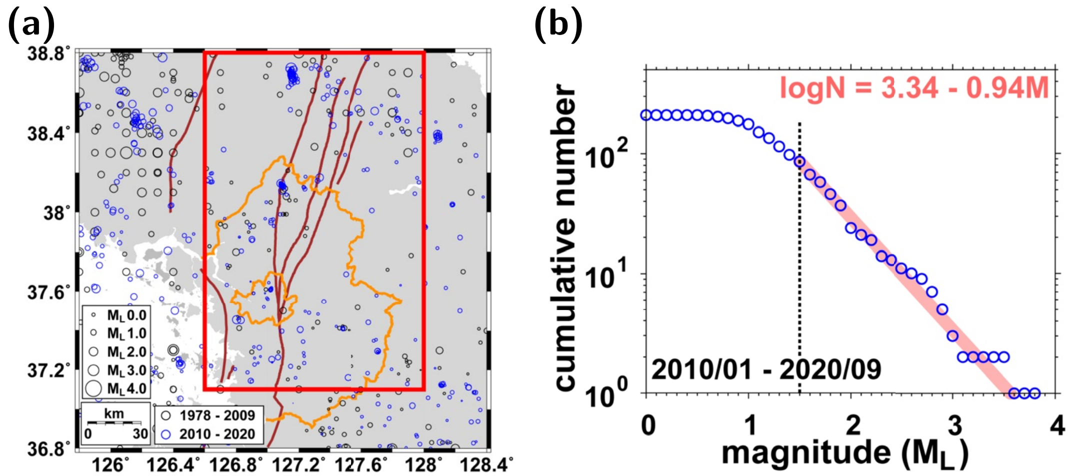

Figure 8. (a) Map of seismicity in the central Korean Peninsula. Major faults (solid lines) and seismicity (circles) are indicated. (b) Estimation of Gutenberg-Richter magnitude-frequency relationship of seismicity in Seoul metropolitan area (boxed region in (a)). The *b* value is 0.94.

orientations are not consistent with the lineament orientations and spatial distribution of earthquakes. The fault-plane orientations agree with the ambient stress field. The fault plane orientations are consistently observed in both normal-faulting and strike-slip events (see events 7 and 9 in region R1).

We find closely located earthquakes such as the September 24, 2018 M_L1.6 earthquake (event 1 in region R1) and the September 21, 2019 M_L3.5 earthquake (event 2) (Figures 12 and 15a). The earthquake occurrence in close locations with a time interval of 1 year may suggest the presence of active earthquake-spawning faults in the region. The June 5, 2009 M_L2.8 earthquake (event 6) occurred in a fault that may be subparallel with the orientation of the northern Pocheon fault.

The May 10, 2019 M_L2.2 earthquake (event 9) was a normal-faulting event that was unusual in the region. The strike was N37°E, consistent with other events in the region. The clustered earthquakes and NE-SW directional fault planes may suggest the presence of earthquake-spawning faults responding to the ambient stress field (Figures 15a and 16).

8.2. Region R2: Central Chugaryeong Fault Zone

A series of earthquakes are clustered in the central Chugaryeong fault zone that is located in the northern Gyeonggi province (region R2; Figure 13). Micro earthquakes occur frequently in the northern region.

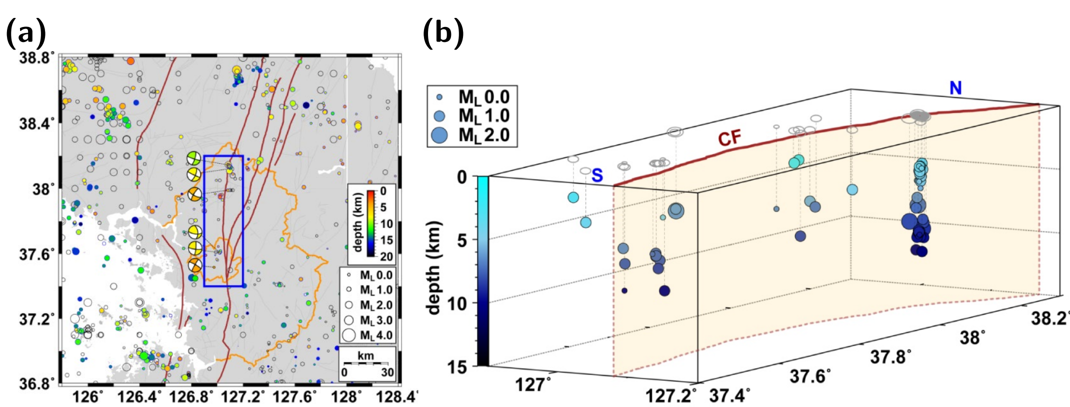

Figure 9. Seismicity distribution around Chugaryeong fault: (a) map view and (b) 3-D view. The 3-D view is presented for the marked region (box). Focal mechanism solutions of earthquakes around Chugaryeong fault are presented. The fault-plane orientations from the focal mechanism solutions are subparallel with the surface fault traces.

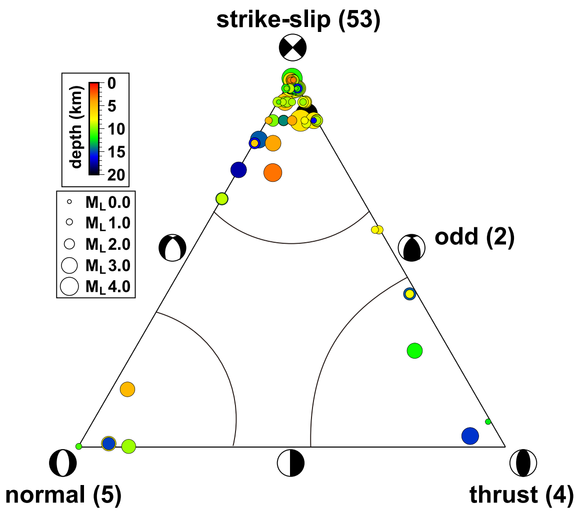

Figure 10. Event type classification of earthquakes in the central Korean Peninsula. Strike-slip faulting is dominant (53 events out of 64 events). Some normal-faulting and thrust events (5 and 4 events) are observed.

Pocheon fault (PF) and Wangsukcheon fault (WF) are located east from Chugaryeong fault (CF), extending to the Seoul metropolitan area. Earthquakes are located around faults. In particular, we observe clustered earthquakes in Yeoncheon, Gyeonggi province where Chugaryeong fault is located (Figures 13 and 15b). The northern CF segment in region R2 is oriented to the NE. The southern CF segment in R2 trends N-S.

Most events were strike-slip earthquakes, except the July 20, 2012 M_L 1.1 earthquake (event 3 in region R2) which presents normal-faulting focal mechanisms. The strike orientations are consistent with the fault trace on the surface. The July 20, 2012 M_L 1.1 earthquake (event 3) in Paju, Gyeonggi province occurred at depth of 12 km.

The Yeoncheon fault segment of Chugaryeong fault is oriented in NE. However, the refined event locations present apparent linear distribution in NW-SE, which is near-orthogonal to the known surface fault traces (Figures 15b and 16a). The earthquakes occurred at depths of 7–8 km. The spatial distribution of earthquakes around Yeoncheon suggests fault planes striking in NW-SE, which is consistent with the fault plane solutions (Figures 15b and 16). The successive faults suggest a possible presence of unknown subsurface active faults that respond to the ambient stress field.

The November 2, 2013 M_L 1.8 earthquake (event 14 in region R2) and the June 28, 2018 M_L 2.7 earthquake (event 13) in Cheolweon present similar strike orientations. The focal depths and strikes are close to those in Yeoncheon. The August 11, 2015 M_L 1.3 earthquake (event 4) in Dongducheon was a strike-slip event. The strike orientation is N49°E. The earthquakes (events 4, 5) in latitudes ≤ 38°N around Chugaryeong fault have focal depths of ∼4 km, which is shallower than those in the northern Chugaryeong fault.

8.3. Region R3: Southern Chugaryeong Fault Zone

Wangsukcheon fault (WF) and Pocheon fault (PF) run across the Seoul metropolitan area (region R3; Figure 14). Chugaryeong fault (CF) is placed across Seoul and to the south. Chugaryeong fault is connected to Singal fault (SF) in the southern Gyeonggi province. Wangsukcheon fault and Pocheon fault converge to Chugaryeong fault in Seoul. We observe that earthquakes are clustered around known faults. The fault-plane orientations follow the ambient stress field. The earthquake distribution in northern Seoul agrees with the fault-plane solutions.

We observe a clustered seismicity in middle-northern Seoul (Figures 14 and 15c). The events are located ∼ 3 km west from the surface lineament. The earthquakes were temporally concentrated in January–March 2019. The magnitudes were M_L1.3–1.5. The focal mechanism solutions are determined among the clustered events. The fault planes are determined to be N7°W–N15°E (events 4–7). The fault-plane orientations are close to the spatial distribution of events (Figures 15c and 16). The clustered events are confined to a narrow depth range of 7.4–8.4 km. The refined event locations based on the double difference method suggests the active fault plane dimension and motion sense. The N-S directional event distribution and strike-slip fault motions of clustered events suggest possible association with the Chugaryeong fault.

There were two consecutive strike-slip earthquakes in December 2019 (events 2, 3) in northwestern Seoul. The earthquakes had strikes in N20°E–N24°E. The focal depths were ∼3 km. We also observe sparsely distributed events around the lineaments east of Seoul (events 8–12).

9. Seismic Implications

The Chugaryeong fault system crosses the Seoul metropolitan area. Earthquakes are located around the fault system. Strike-slip motions are dominant in the fault system. It is known that ambient stress field is a dominant factor to control fault-plane orientations and fault slips (Zoback & Zoback, 1980). The orienta-

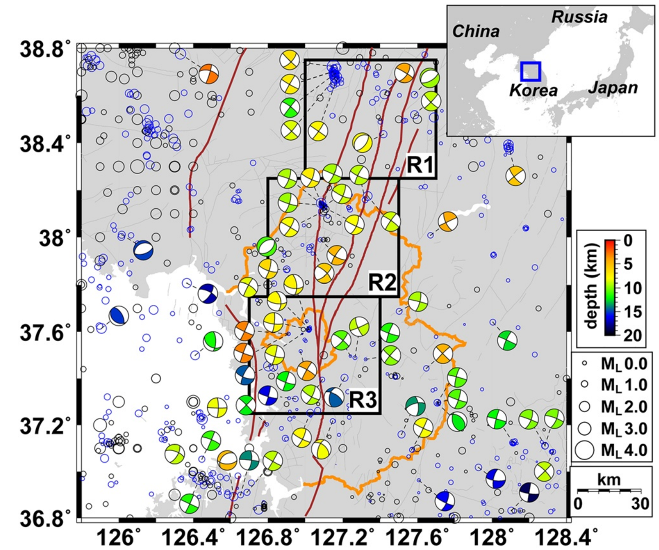

Figure 11. Spatial distribution of focal mechanism solutions and seismicity. Three subregions (R1, R2, R3) are marked along the Chugaryeong fault system. Strike-slip events are dominant.

tion of primary compressional field from the focal mechanism solutions is consistent with the ambient stress field (S.-J. Choi, et al., 2012; J. Lee et al., 2017; Zoback, 1992). The seismicity suggests development of fault segments satisfying the ambient stress field.

The ambient stress produces strike-slip faults striking in NE-SW, which is widely in the Korean Peninsula (S.-J. Choi, et al., 2012; J. Lee et al., 2017). The observation suggests that faults may extend according to the ambient stress field. The earthquakes in middle-northern Seoul, however, present N-S directional fault-plane orientations that are subparallel with the lineament of Chugaryeong fault. The apparent motion suggests that the earthquakes may be associated with Chugaryeong fault.

Chugaryeong fault exhibits bending, which may suggest the connection of fault segments. The fault structures develop from the bending locations, where the stress accumulation may be locally maximized. However, the N-S directional fault plane and seismicity suggest that the NE-SW directional fault structures may respond continuously, subsequently deforming the adjacent media. This observation indicates that the fault structures are connected with each other, responding to the ambient stress over the whole fault system. The source mechanisms (N-S directional strike-slip events and NE-SW directional strike-slip events) and connection of fault structures suggest that the faults are segmented but may be connected and respond continuously.

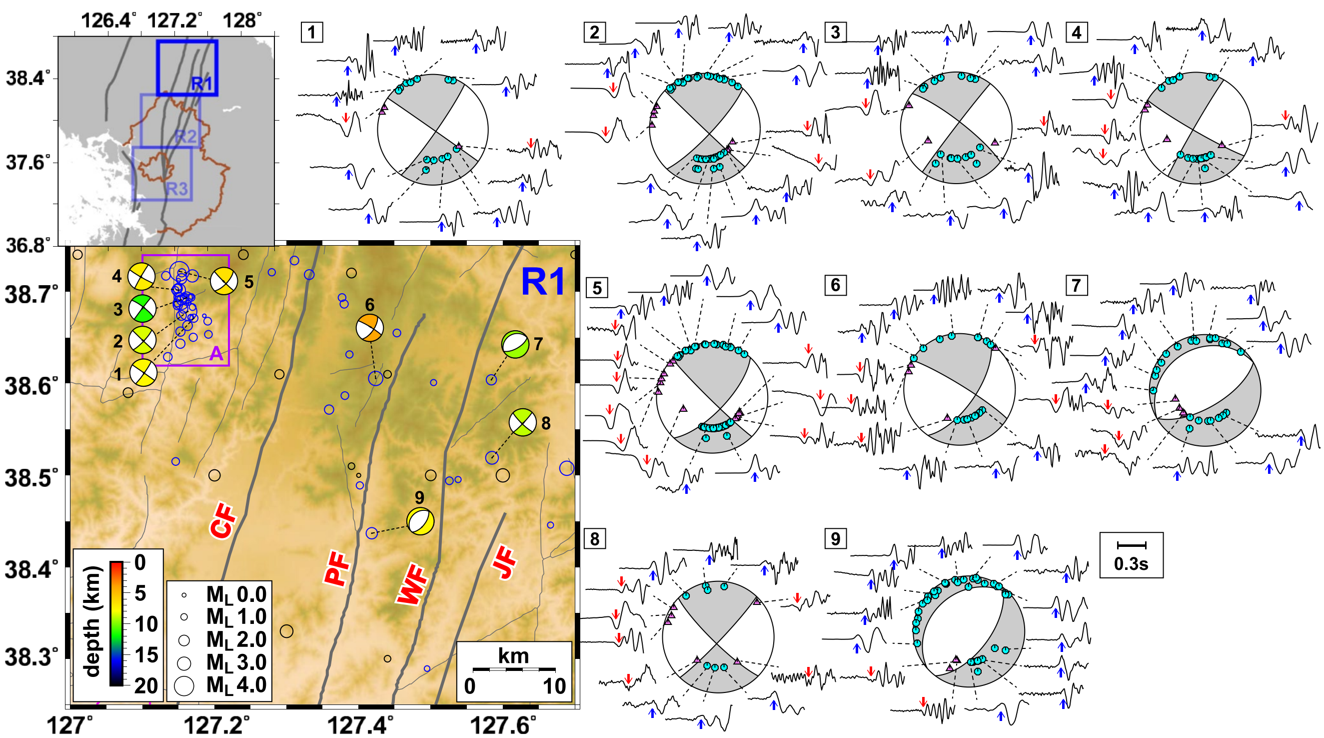

Figure 12. Enlarged seismicity map of region R1. The focal mechanism solutions and waveforms of events are presented. The events include the September 24, 2018 M_L 1.6 earthquake (event 1), the September 21, 2019 M_L 3.5 earthquake (event 2), the October 12, 2018 M_L 2.3 earthquake (event 3), the January 29, 2017 M_L 2.6 earthquake (event 4), the May 11, 2020 M_L 3.8 earthquake (event 5), the June 05, 2009 M_L 2.8 earthquake (event 6), the April 21, 2019 M_L 2.0 earthquake (event 7), the March 11, 2011 M_L 2.5 earthquake (event 8), and the May 10, 2019 M_L 2.2 earthquake (event 9). Major fault traces are denoted (CF, PF, WF, and JF).

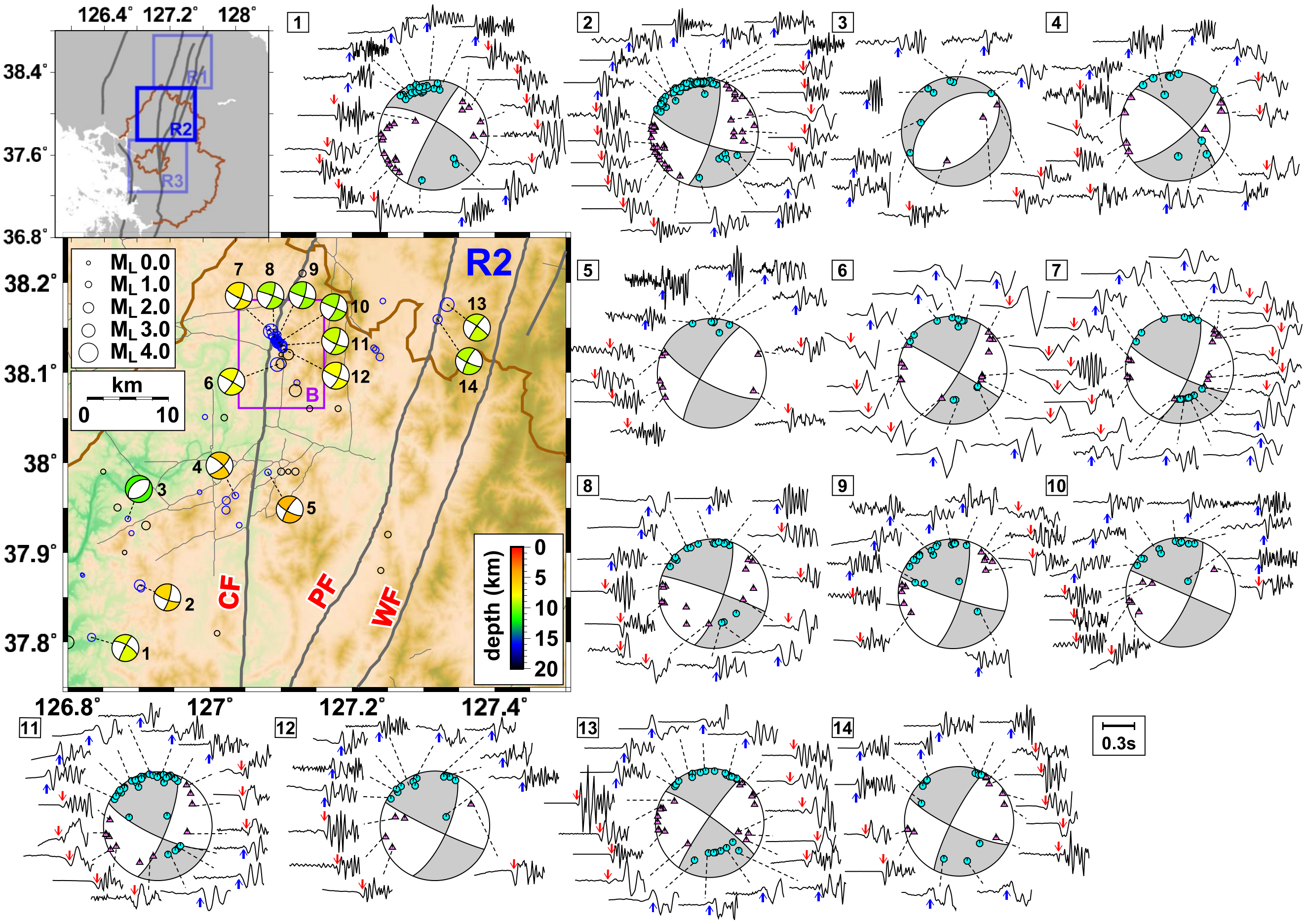

Figure 13. Enlarged seismicity map of region R2. The focal mechanism solutions and waveforms of selected events are presented. The selected events include the September 4, 2020 M_L 1.6 earthquake (event 1), the June 23, 2020 M_L 2.1 earthquake (event 2), the July 20, 2012 M_L 1.1 earthquake (event 3), the August 11, 2015 M_L 1.3 earthquake (event 4), the November 26, 2018 M_L 1.3 earthquake (event 5), the March 26, 2009 M_L 2.7 earthquake (event 6), the December 19, 2013 M_L 2.9 earthquake (event 7), the March 24, 2017 M_L 1.9 earthquake (event 8), the September 25, 2019 M_L 1.2 earthquake (event 9), the September 17, 2019 M_L 1.3 earthquake (event 10), the September 10, 2019 M_L 2.0 earthquake (event 11), the November 8, 2019 M_L 1.3 earthquake (event 12), the June 28, 2018 M_L 2.7 earthquake (event 13), and the November 2, 2013 M_L 1.8 earthquake (event 14). Major fault traces are denoted (CF, PF, and WF).

The continuous connection and interaction between segments may produce continuous and successive deformation over the Chugaryeong fault system. The observation supports that the fault system is completely connected. The observation suggests that the Chugaryeong fault system may be a primary fault system in the Korean Peninsula. The dominant earthquake occurrence is observed arising from the Chugaryeong fault.

10. Discussion and Conclusions

The Korean Peninsula is placed in a stable intraplate region with relatively low earthquake occurrence rates compared to active plate-boundary regions. Thus, the Korean Peninsula exhibits relatively long earthquake recurrence times. The central Korean Peninsula, in particular, belongs to the Gyeonggi massif, where the seismicity is low according to the instrumental earthquake records. The region is stable, requiring long accumulation of stress to induce large or moderate-size earthquakes. Quaternary faults are located across the Seoul metropolitan area, where the population is high.

However, large seismic damages were historically reported. In particular, major historical earthquakes are placed around Chugaryeong fault system. Further, the seismicity of the Korean Peninsula increased after the 2011 M_W9.0 Tohoku-Oki megathrust earthquake. A series of moderate-size earthquakes, including the

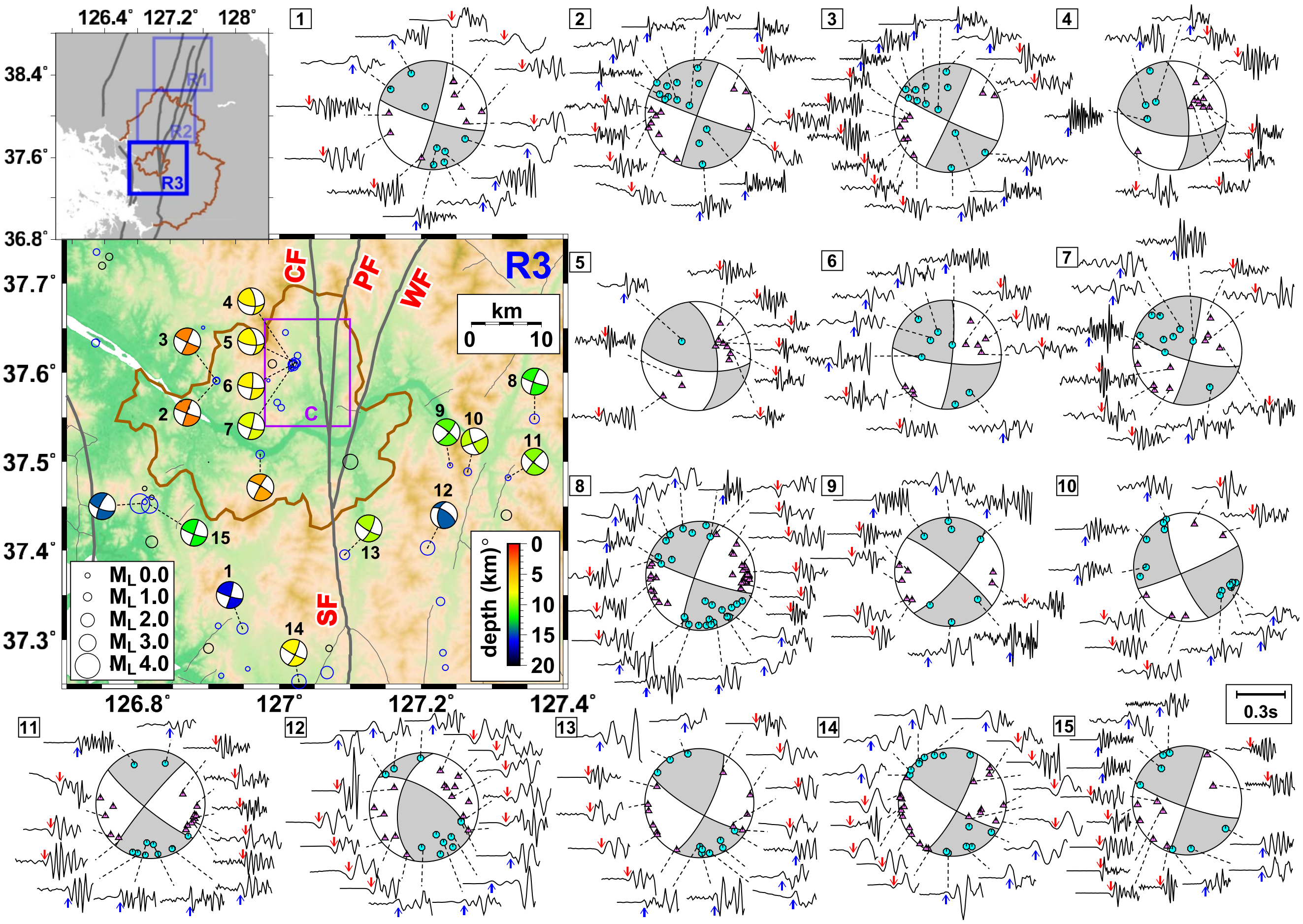

Figure 14. Enlarged seismicity map of region R3. The focal mechanism solutions and waveforms of selected events are presented. The selected events include the April 4, 2017 M_L 1.7 earthquake (event 1), the December 5, 2019 M_L 1.1 earthquake (event 2), the December 5, 2019 M_L 1.0 earthquake (event 3), the January 29, 2019 M_L 1.5 earthquake (event 4), the February 5, 2019 M_L 1.3 earthquake (event 5), the March 20, 2019 M_L 1.5 earthquake (event 6), the March 19, 2019 M_L 1.5 earthquake (event 7), the April 10, 2020 M_L 1.5 earthquake (event 8), the July 14, 2019 M_L 0.8 earthquake (event 9), the January 7, 2019 M_L 1.2 earthquake (event 10), the July 16, 2019 M_L 0.9 earthquake (event 11), the August 1, 2014 M_L 2.2 earthquake (event 12), the October 8, 2010 M_L 1.5 earthquake (event 13), and the October 24, 2016 M_L 2.2 earthquake (event 14). Major fault traces are denoted (CF, PF, SF, and WF).

2016 M_L5.8 Gyeongju earthquake, occurred after the Tohoku-Oki earthquake. There were concerns about possible occurrences of large earthquakes in the central Korean Peninsula.

We investigated the seismicity and fault structures in the Seoul metropolitan area from spatial distribution and source mechanisms of earthquakes that were recorded in dense seismic networks. We refined 455 earthquake source parameters. We determined the focal mechanism solutions of 64 earthquakes in Seoul metropolitan area in 2004–2020 using the polarity of phase and S/P amplitude ratios. The fault plane analyses of earthquakes present the fault geometry and slip sense. We could infer the local distribution of active faults from the seismicity and focal mechanism solutions.

Strike-slip earthquakes are dominant in the central Korean Peninsula. Fractional earthquakes presented reverse and normal-faulting mechanisms. The dominant focal depths are 4–15 km. The compressional stress orientations from the focal mechanism solutions are generally consistent with the ambient stress field in the region. The observation suggests that the ambient stress field combining lithostatic stress from convergent plate margins and local stress perturbation by local geological properties may control the fault-slip motions and fault-plane orientations dominantly.

The refined earthquakes are clustered around the Chugaryeong fault system. The seismicity generally lies on the source regions of major historical earthquakes. The earthquakes in the northern Seoul metropolitan

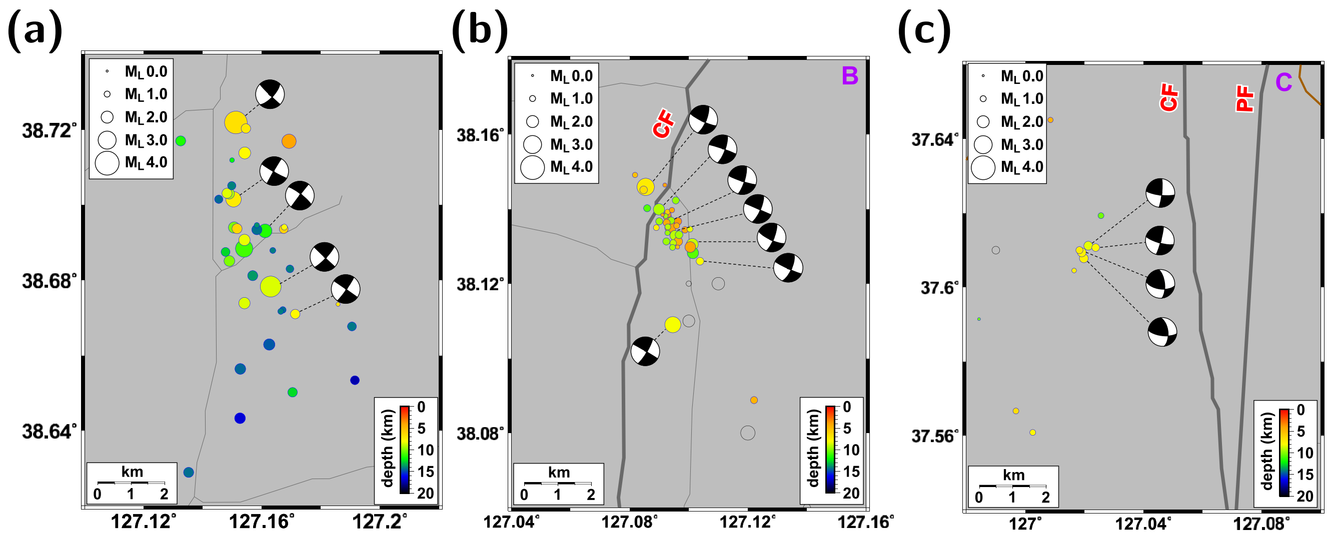

Figure 15. Enlarged map of high seismicity regions: (a) A in region R1, (b) B in region R2, and (c) C in region R3. The earthquakes are clustered in small regions. Major faults and surface lineaments are presented (solid lines).

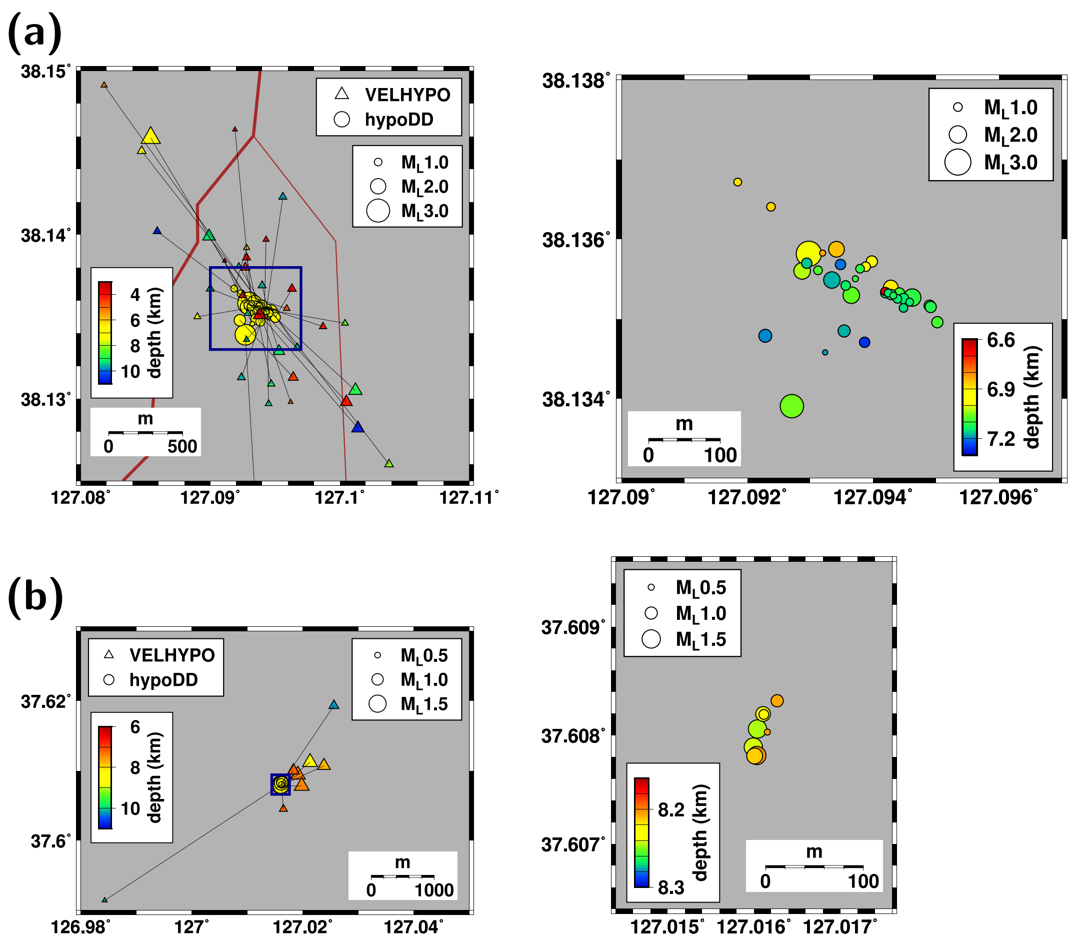

Figure 16. Earthquake relocation based on double-difference method: (a) B in region R2, and (b) C in region R3, (left) comparison between original locations and refined locations, and (right) map view of refined locations. The events are clustered in small areas.

area present fault plane solutions with strikes orienting in NNE-SSW (N20°E–N30°E). The earthquakes in the central Seoul metropolitan area present NNE-SSW to N-S fault strikes (N7°E–N15°E). The earthquakes in the southern Seoul metropolitan area present NNE-SSW fault strikes (N20°E–N30°E). The observation suggests that many locations of Chugaryeong fault system have posture and geometry conforming to the current ambient stress field.

The fault plane solutions of the earthquakes in Pyeongang, Kangwon province (region R1), Yeoncheon Gyeonggi province (region R2), and Seongbuk-gu, Seoul (region R3) are nearly subparallel with the surface traces of Chugaryeong fault. However, the spatial distribution of refined seismicity suggests that the clustered earthquakes in Yeoncheon (region R2) occur on fault planes striking in NW-SE. The auxiliary planes of focal mechanism solutions for the clustered earthquakes are subparallel with the Chugaryeong fault traces. The observation suggests that the Chugaryeong fault may be branched locally, responding to the ambient stress field.

A series of micro-to-small strike-slip earthquakes occurred in middle-northern Seoul (Seongbuk-gu, region R3). The spatial distribution of earthquakes and focal mechanism solutions agrees with the fault traces on the surface (lineaments in N-S). The observation suggests N-S directional near-vertical active faults in the region.

According to the focal mechanism solutions and surface lineaments, it appears that the fault-plane orientation changes along Chugaryeong fault. The resolved strikes of fault planes or auxiliary plane are subparallel with the surface fault trace. The observation suggests that Chugaryeong fault may behave as a backbone fault to accommodate locally active fault segments or fault branches. Also, the observation may indicate that the Chugaryeong fault may be connected along the surface traces. The whole fault system, fault segmentation, and potential faulting dimensions may be resolved through geological, and explorational seismic and geophysical surveys.

Data Availability Statement

The full event list and data sets are available on Dryad (https://doi.org/10.5061/dryad.69p8cz926).

Acknowledgments
We are grateful to Dr. Andrea Donnellan (editor) and anonymous reviewer for valuable comments. The seismic records were collected from the Korean Meteorological Administration (KMA) and Korea Institute of Geoscience and Mineral Resources (KIGAM). This work was supported by the Korea Meteorological Administration Research and Development Program under grant KMI2018-02910. Additionally, this research was partly supported by the Basic Science Research Program of the National Research Foundation of Korea (NRF-2017R1A6A1A07015374, NRF-2018R1D1A1A09083446).

References

Bae, H.-K., & Lee, H.-K. (2016). Quaternary activity patterns of the Wangsukcheon Fault in the Pocheon-Namyangju area, Korea (in Korean with English abstract). *Journal of the Geological Society of Korea*, *52*(2), 129–147. https://doi.org/10.14770/jgsk.2016.52.2.129

Choi, H., Hong, T.-K., He, X., & Baag, C.-E. (2012). Seismic evidence for reverse activation of a paleo-rifting system in the East Sea (Sea of Japan). *Tectonophysics*, *572–573*, 123–133. https://doi.org/10.1016/j.tecto.2011.12.023

Choi, S.-J., Chwae, U., Lee, H.-K., Song, Y., & Kang, I.-M. (2012). Review on the Chugaryeong Fault (in Korean with English abstract). *Journal of Korean Society of Economic and Enviromental Geology*, *45*(4), 441–446. https://doi.org/10.9719/eeg.2012.45.4.441

Chough, S. K., Kwon, S.-T., Ree, J.-H., & Choi, D. K. (2000). Tectonic and sedimentary evolution of the Korean peninsula: A review and new view. *Earth-Science Reviews*, *52*(1–3), 175–235. https://doi.org/10.1016/s0012-8252(00)00029-5

Chung, D., Song, Y., Park, C., Kang, I.-M., Choi, S.-J., Khulganakhuu, C., & Khulganakhuu, C. (2014). Reactivated timings of some major faults in the Chugaryeong Fault Zone since the cretaceous period (in Korean with English abstract). *Journal of Korean Society of Economic and Enviromental Geology*, *47*(1), 29–38. https://doi.org/10.9719/eeg.2014.47.1.29

Frohlich, C., & Apperson, K. D. (1992). Earthquake focal mechanisms, moment tensors, and the consistency of seismic activity near plate boundaries. *Tectonics*, *11*(2), 279–296. https://doi.org/10.1029/91tc02888

Gutenberg, B., & Richter, C. F. (1956). Earthquake magnitude, intensity, energy, and acceleration (Second paper). *Bulletin of the Seismological Society of America*, *46*, 105–145. https://doi.org/10.1785/bssa0460020105

Hanks, T. C., & Kanamori, H. (1979). A moment magnitude scale. *Journal of Geophysical Research*, *84*, 2348–2350. https://doi.org/10.1029/jb084ib05p02348

He, X., & Hong, T.-K. (2010). Evidence for strong ground motion by waves refracted from the Conrad discontinuity. *Bulletin of the Seismological Society of America*, *100*(3), 1370–1374. https://doi.org/10.1785/0120090159

Hong, T.-K., Baag, C.-E., Choi, H., & Sheen, D.-H. (2008). Regional seismic observations of the October 9, 2006 underground nuclear explosion in North Korea and the influence of crustal structure on regional phases. *Journal of Geophysical Research*, *113*, B03305. https://doi.org/10.1029/2007JB004950

Hong, T.-K., & Choi, H. (2012). Seismological constraints on the collision belt between the North and South China blocks in the Yellow Sea. *Tectonophysics*, *570–571*, 102–113. https://doi.org/10.1016/j.tecto.2012.08.034

Hong, T.-K., Lee, J., & Houng, S. E. (2015). Long-term evolution of intraplate seismicity in stress shadows after a megathrust. *Physics of the Earth and Planetary Interiors*, *245*, 59–70. https://doi.org/10.1016/j.pepi.2015.05.009

Hong, T.-K., Lee, J., Kim, W., Hahm, I.-K., Woo, N.-C., & Park, S. (2017). The 12 September 2016 M_L5.8 midcrustal earthquake in the Korean Peninsula and its seismic implications. *Geophysical Research Letters*, *44*, 3131–3138. https://doi.org/10.1002/2017gl072899

Hong, T.-K., Lee, J., Park, S., & Kim, W. (2018). Time-advanced occurrence of moderate-size earthquakes in a stable intraplate region after a megathrust earthquake and their seismic properties. *Scientific Reports*, *8*, 13331. https://doi.org/10.1038/s41598-018-31600-5
Hong, T.-K., Park, S., & Houng, S. E. (2016). Seismotectonic properties and zonation of the far-eastern Eurasian plate around the Korean Peninsula. *Pure and Applied Geophysics*, *173*(4), 1175–1195. https://doi.org/10.1007/s00024-015-1170-2
Hong, T.-K., Park, S., Lee, J., Chung, D., & Kim, W. (2020). One-off deep crustal earthquake swarm in a stable intracontinental region of the southwestern Korean Peninsula. *Physics of the Earth and Planetary Interiors*, *308*, 106582. https://doi.org/10.1016/j.pepi.2020.106582
Hong, T.-K., Park, S., Lee, J., & Kim, W. (2020). Spatiotemporal seismicity evolution and seismic hazard potentials in the western East Sea (Sea of Japan). *Pure and Applied Geophysics*, *177*(8), 3761–3774. https://doi.org/10.1007/s00024-020-02479-z
Houng, S. E., & Hong, T.-K. (2013). Probabilistic analysis of the Korean historical earthquake records. *Bulletin of the Seismological Society of America*, *103*(5), 2782–2796. https://doi.org/10.1785/0120120318
Kennett, B. L. N., Engdahl, E. R., & Buland, R. (1995). Constraints on seismic velocities in the Earth from traveltimes. *Geophysical Journal International*, *122*(1), 108–124. https://doi.org/10.1111/j.1365-246x.1995.tb03540.x
Kim, O. J. (1973). The Straigraphy and geologic structure of the metamorphic complex in the Northwestern Area of the Kyonggi Massif (in Korean with English abstract). *Journal of Korean Society of Economic and Enviromental Geology*, *6*, 201–218.
Kim, S., Rhie, J., & Kim, G. (2011). Forward waveform modelling procedure for 1-D crustal velocity structure and its application to the southern Korean Peninsula. *Geophysical Journal International*, *185*(1), 453–468. https://doi.org/10.1111/j.1365-246x.2011.04949.x
Kim, W., Hong, T.-K., & Kang, T. S. (2014). Hypocentral parameter inversion for regions with poorly known velocity structures. *Tectonophysics*, *627*, 182–192. https://doi.org/10.1016/j.tecto.2013.06.024
Kim, W., Hong, T.-K., Lee, J., & Taira, T. A. (2016). Seismicity and fault geometry of the San Andreas fault around Parkfield, California and their implications. *Tectonophysics*, *677*, 34–44. https://doi.org/10.1016/j.tecto.2016.03.038
Kyung, J. B. (2012). Characteristics of damaging earthquakes occurred in Seoul metropolitan area for the last two thousand years (in Korean with English abstract). *Journal of the Korean Earth Science Society*, *33*(7), 637–644. https://doi.org/10.5467/jkess.2012.33.7.637
Lee, J., Hong, T.-K., & Chang, C. (2017). Crustal stress field perturbations in the continental margin around the Korean Peninsula and Japanese islands. *Tectonophysics*, *718*, 140–149. https://doi.org/10.1016/j.tecto.2017.08.003
Lee, K., & Yang, W. (2006). Historical seismicity of Korea. *Bulletin of the Seismological Society of America*, *96*, 846–855. https://doi.org/10.1785/0120050050
Mayeda, K., Hofstetter, A., O'Boyle, J. L., & Walter, W. R. (2003). Stable and transportable regional magnitudes based on coda-derived momentrate spectra. *Bulletin of the Seismological Society of America*, *93*, 224–239. https://doi.org/10.1785/0120020020
Mayeda, K., & Walter, W. R. (1996). Moment, energy, stress drop, and source spectra of western United States earthquakes from regional coda envelopes. *Journal of Geophysical Research*, *101*(11), 11195–11208. https://doi.org/10.1029/96jb00112
Park, S., Baek, I., & Hong, T.-K. (2020). Six major historical earthquakes in the Seoul metropolitan area during the Joseon dynasty (1392-1910). *Bulletin of the Seismological Society of America*, *110*(6), 3037–3049. https://doi.org/10.1785/0120200004
Pearthree, P. A., & Calvo, S. S. (1987). The Santa Rita fault zone: Evidence for large magnitude earthquakes with very long recurrence intervals, Basin and Range province of southeastern Arizona. *Bulletin of the Seismological Society of America*, *77*, 97–116.
Schwartz, D. P., & Coppersmith, K. J. (1984). Fault behavior and characteristic earthquakes: Examples from the Wasatch and San Andreas fault zones. *Journal of Geophysical Research*, *89*, 5681–5698. https://doi.org/10.1029/jb089ib07p05681
Shimazaki, K., & Nakata, T. (1980). Time-predictable recurrence model for large earthquakes. *Geophysical Research Letters*, *7*, 279–282. https://doi.org/10.1029/gl007i004p00279
Snoke, J. A. (2003). FOCMEC: Focal mechanism determinations. In W. H. K. Lee, H. Kanamori, P. C. Jennings, & C. Kisslinger (Eds.), International handbook of earthquake and engineering seismology. Academic Press.
Waldhauser, F., & Ellsworth, W. L. (2000). A double-difference earthquake location algorithm: Method and application to the northern Hayward fault, California. *Bulletin of the Seismological Society of America*, *90*, 1353–1368. https://doi.org/10.1785/0120000006
Withers, M., Aster, R., Young, C., Beiriger, J., Harris, M., Moore, S., & Trujillo, J. (1998). A comparison of select trigger algorithms for automated global seismic phase and event Detection. *Bulletin of the Seismological Society of America*, *88*(1), 95–106.
Yoo, S.-H., Rhie, J., Choi, H., & Mayeda, K. (2011). Coda-derived source parameters of earthquakes and their scaling relationships in the Korean Peninsula. *Bulletin of the Seismological Society of America*, *101*(5), 2388–2398. https://doi.org/10.1785/0120100318
Zoback, M. L. (1992). First-and second-order patterns of stress in the lithosphere: The World Stress Map Project. *Journal of Geophysical Research*, *97*(B8), 11703–11728. https://doi.org/10.1029/92jb00132
Zoback, M. L., & Zoback, M. (1980). State of stress in the conterminous United States. *Journal of Geophysical Research*, *85*(B11), 6113–6156. https://doi.org/10.1029/jb085ib11p06113